Leading Edge Vortex Formation on a Flapping Wing Robotic Bird

L.H. Groot Koerkamp*, H.W.M. Hoeijmakers †, C.H. Venner‡ and S. Stramigioli §
University of Twente, Enschede, the Netherlands

The Robird is an bird-like drone that flies by flapping its wings. It closely resembles a peregrine falcon in appearance, size and weight, but more specifically in its flapping flight performance. Drones like the Robird could might useful purposes such as bird control at airports, but their development is currently hampered by a limited understanding of the aerodynamics involved. The present study aims to identify the role of attached vortical structures on the flight performance of the Robotic bird. Particle Tracking Velocimetry (PTV) measurements were performed on a relatively large volume ($200\,\mathrm{mm} \times 500\,\mathrm{mm} \times 600\,\mathrm{mm}$) **around the flapping Robird wing. The measurement data shows two significant attached vortical structures: one on the lower side of the wing during the upstroke, and a smaller one on the upper side of the wing during the downstroke. The vortex on the lower side is accompanied by significant spanwise flow near the wing surface. The magnitude of this spanwise flow depends on the Strouhal number, which is a dimensionless measure for the flapping frequency.**

I. Introduction

The Robird [1] is an ornithopter-type drone that generates thrust and lift using flapping wings only. It has been developed by a spin-off company of the University of Twente, and it was designed to look like a peregrine falcon during its flight, as seen in Fig. 1. The Robird has been used successfully for bird control at airports and garbage dumps. Ideally when developing a bio-inspired robot, one applies lessons learned from nature. Two successful examples of this bio-inspired engineering process are the Delfly [2] and the Robobee [3]. When the Robird was first developed, this bio-inspired approach was only applicable to a limited extent since the majority of available literature focused on insects. Even though there is an overlap in Strouhal number between birds of any size and large insects [4], the Reynolds number has a different order of magnitude. Because of this, there is a significant knowledge gap between the flapping wing aerodynamics of large ornithopters (i.e. the Robird, the Festo Smart Gull [5], the Robo Raven [6]) and smaller ones such as the Robobee.

It has been well-established that Leading Edge Vortices (LEV's) play an important role in the generation of lift for insects [7, 8]. These vortices are typically stable, which can be attributed to the angular acceleration of the fluid induced by the flapping motion of a wing [9]. The phenomenon of LEV's has been studied more thoroughly for insects than for birds and bats [10]. More recently in-vivo measurements have revealed LEV's in vertebrates as well. Particle Image Velocimetry (PIV) measurements on hovering hummingbirds [11] and slow-flying pied flycatchers (small birds) [12] showed these lift-enhancing vortical flow structures on the wings of both sorts of birds. From an energy perspective, one would expect the LEV to be a transitional phenomenon between forward and hovering flight. Exactly this has been confirmed for small bats (lesser long-nosed bats) [13]. A contradicting result was found on a flapping model of a goose, where LEV's were also found for cruise conditions [14]. Numerical work (2D uRANS) for an oscillating Robird airfoil shows similar results [15]. Experimental work on the Robird, however, has mainly focused on the wake [16, 17].

Previous research on an insect scale could benefit from powerful particle based measurement methods such as tomographic Particle Image Velocimetry (PIV). With commonly used micrometer-sized seeding, the maximum interrogation volume achievable in air is approximately $50\,\mathrm{cm}^3$ [18]. This is perfect for insect-scale flows, but too small for the flow around larger birds. A novel solution to this issue is using Helium-Filled Soap Bubble seeding. Helium-Filled Soap Bubbles (abbreviated as HFSB) are significantly more reflective than commonly used oil-droplet seeding in wind tunnels [19]. This allows for an increase of interrogation volume size of three orders of magnitude

*PhD Student, Department Electrical Engineering, Mathematics and Computer Sciences, PO Box 217, 7500 AE Enschede, the Netherlands. Student Member AIAA

†Professor, Faculty Engineering Technology, PO Box 217, 7500 AE Enschede, the Netherlands. Senior Member AIAA.

‡Professor, Faculty Engineering Technology, PO Box 217, 7500 AE Enschede, the Netherlands. Member AIAA.

§Professor, Faculty Electrical Engineering, Mathematics and Computer Sciences, PO Box 217, 7500 AE Enschede, the Netherlands

Fig. 1 The Robird [1]

[20]. In addition, a newly developed PTV method called Shake-The-Box has become commercially available [21]. This method allows for volumetric analysis of flows with seeding densities as high as 0.125 ppp (particles per pixel) [22]. These two developments have paved the way for new measurements on the flow about birds that could bridge the gap between insect scale research and bird scale research.

In the present study, a wing flapping device resembling the port-side of the Robird was placed in a half open wind tunnel section. The flow was seeded with HFSB. Four high-speed cameras acquired images of the flapping wing at a rate of 2 kHz, resulting in time-resolved data. The novel Shake-The-Box algorithm was used to calculate particle tracks. These tracks were plotted and colored according to the local normalized velocity magnitude or normalized spanwise velocity.

The objective of the present study is to identify vortical structures around the flapping wing of a Robird in cruise flight conditions. The Robird provides an excellent research platform since it is a configuration that has proven to be able to fly in a natural environment.

The present work is structured as follows: In section II the materials and method of this research are described. In section III some first results are presented. Section IV gives the main conclusions of this research and provides an outlook to future work.

II. Materials and Method

The wind-tunnel model has been designed to match the exterior shape of the portside of the Robird wing and fuselage. The model does not include the tail of the Robird. A standard Robird wing was connected to the flapping device via the two main spars that run along the span of the Robird wing as seen in Fig. 3b. Contrary to the design of the Robird, each spar is driven by its own brushless DC motor (Fig. 3a). The wing has a half-span from wing root to wing tip of 520 mm. The device can flap 30° downward and 45° upwards. The setup was placed in the half-open test section of the University of Twente Aeroacoustic Wind Tunnel [23] (width 0.9 m, height 0.7 m). The wing is somewhat large for this test section, so interactions between wing aerodynamics and the wall and/or jet shear layer are to be expected. This was accepted because the trade-off guaranteed similarity in aeroealastic behaviour of the wing, which is believed to play a significant role in the flight characteristics of the Robird.

The flapping device has a maximum flapping frequency of 3 Hz. Since turbulence levels of the wind tunnel are unknown for speeds lower than 5 m/s, a velocity of 6 $ms^{-1}$was taken as the lower limit for the velocity of the air stream. The experiment matrix is given in Table 1. In this table, the Strouhal number and the Reynolds number are listed. These

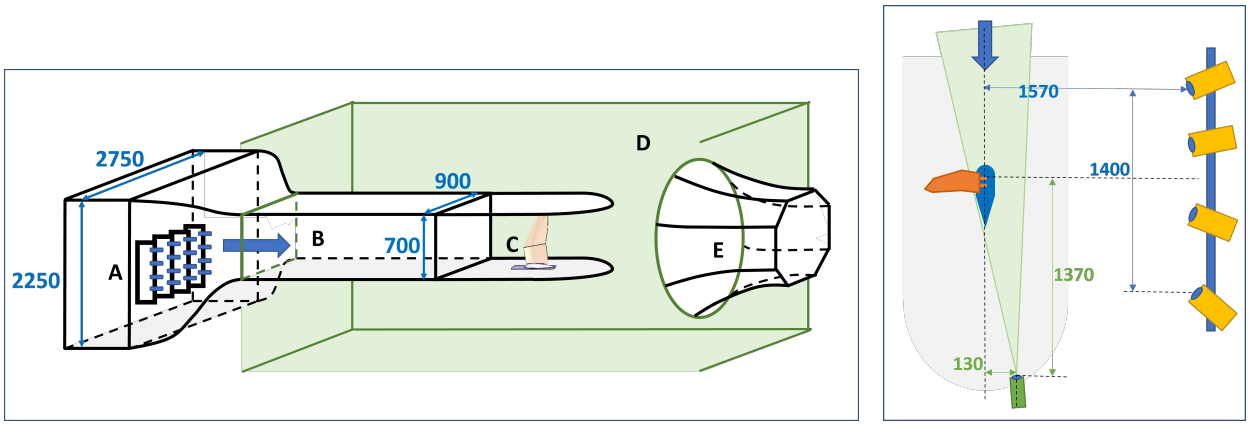

(a) (b)

Fig. 2 (a) Overview of University of Twente Aeroacoustic Wind Tunnel. The HFSB nozzles, mounted on 4 arrays per 20 , are shown at point A. The flapping wing model is not drawn to scale and shown at location C.(b) Top view of flapping device in half-open section of wind tunnel. Camera's are shown in yellow, wing in orange and illuminated volume in green. All dimensions are given in mm.

Table 1 Matrix of all experiments and their parameters

U_∞ [m/s]	$f[Hz]$	St	Re
6	3	0.33	$6.9 \cdot 10^4$
8	3	0.24	$8.5 \cdot 10^4$
10	3	0.19	$1.08 \cdot 10^5$

variables are defined as:

$$\mathrm{St} = \frac{f \cdot (2A)}{U_\infty} \tag{1}$$

$$\mathrm{Re} = \frac{\rho_\infty U_\infty \bar{c}}{\mu_\infty} \tag{2}$$

respectively, with f the flapping frequency in Hz, $2A$ equal two times the amplitude of the wing tip, U_∞ is the free-stream velocity, ρ_∞ and μ_∞ air density and viscosity of the air and $\bar{c}$ the average chord of the Robird wing. The Strouhal numbers achievable are within the relevant range of 0.2 <St< 0.4 [4]. However, to stay in this range a compromise had to be made on the Reynolds number. The Reynolds number could not be varied independently of the Strouhal number.

The flow was seeded with HFSB of approximately 300 μm in diameter by 80 nozzles in the settling chamber of the wind tunnel. The seeded volume that could be achieved was approximately 500 mm high, 200 mm deep and 600 mm wide. The interrogation volume depth is smaller than the maximal excursion of the wing, which is 630 mm. By moving the seeding generator laterally between wind-tunnel entries, the full stroke could be measured in just two volumes. The seeding density achieved was approximately 0.12 ppp.

Four high speed cameras (2 Phantom V611, 2 phantom VEO 710L) were mounted next to the open section in an in-line configuration with an opening angle β of approximately 50 °. The measurement volume was illuminated by a ND-YLF laser at a repetition frequency of 2 kHz. The coherent beam was guided to the downstream portion of the wind-tunnel with a LaVision articulated optical arm. Finally, the laser light beam was transformed into a cone with the help of volume forming optics, which conisted of a variable zoom lens and a concave $f = -50$ mm lens. The measurement volume had a size of 200 mm × 500 mm × 600 mm (depth, height, width). The placement of the camera's and laser optics can be seen in Fig. 2b.

To perform measurements on the upper side of the flapping Robird wing, the flapping mechanism was rotated 180 degrees around its span axis and a starboard Robird wing was mounted on the flapping mechanism. The kinematics of the movement remain similar, however, it should be noted that the aerodynamic shield faced backwards, as shown in Fig. 3c. This may affect the airflow in the root region of the wing.

Fig. 3 (a) A 3D model of the flapping device used in this study, including a model of the Robird wing. (b) Two Robird wings. The unpainted version on the right shows the placement of the leading and trailing edge spars. (c) A starboard side wing mounted backwards on the wing flapping mechanism.

The data was acquired and processed with LaVision's DaVis 10.1 software package. All data was pre-processed with a temporal subtract-time filter with a filter length of 5 images. Subsequently, a local normalization filter and sliding minimum filter were applied. The Shake-The-Box tracking algorithm [22] was used to find suitable particle tracks. In the cases for which particle tracks were converted to vector fields on a structured grid, a binning strategy was used. The volume was subdivided in sub-volumes of 32 voxels × 32 voxels with a 50% overlap, and a voxel is 2 mm^3. Them minimum required amount of particles within a sub-volume was set to two. The velocity in each grid point was calculated with a Gaussian weighing function.

The vector fields were used to derive the λ_2-criterion to assist vortex identification when the tracks themselves did not clearly show vortical structures. This metric identifies vortex cores even with an added convective velocity component in the velocity field [24].

III. Results and Discussion

The most notable feature identified in all experiments is an attached vortical structure that forms at the lower side of the wing during the upstroke. Near this structure the fluid gains a significant velocity component in the spanwise direction. As illustrated in Fig. 4, the relative magnitude of this flow is proportional to the Strouhal number, where $\bar{U}_s pan$ increases for increasing Strouhal number. The cross-sectional images in Fig. 5 show that the structure starts near the end of the arm-wing section of the wing, and increases in size proportionally with the distance from the root. Near the end of the upstroke, this structure detaches or breaks down in all cases.

A secondary feature can be found on the upper side of the wing. This was particularly easy to spot for St=0.24. The three cross-sections in Fig. 6 show that the flow does not remain attached over the entire span during the downstoke of the wing. In this case however it is less clear if a vortical structure is present. For further clarification, iso-surfaces of the lambda-2 criterion are plotted in Fig. 7 This indicates that the vortical structure detaches before reaching the wing-tip. However, it should be noted that hardly any particles were tracked at the tip, so conclusions from this figure should be drawn with appropriate reserve. In addition one should note that this structure could not be observed for St = 0.33.

Both structures appear to be the same phenomenon, despite being on opposite sides of the wing. The LEV is defined as an attached vortical structure that appears beyond the static stall angle of attack. Both structures fit this definition. However, it is important to note some differences between the two. The upper side structure features a clearly discernible area of reversed flow nearest to the wing surface. This cannot be observed on the upper surface of the wing. In addition, the structure on the upper surface of the wing is significantly smaller.

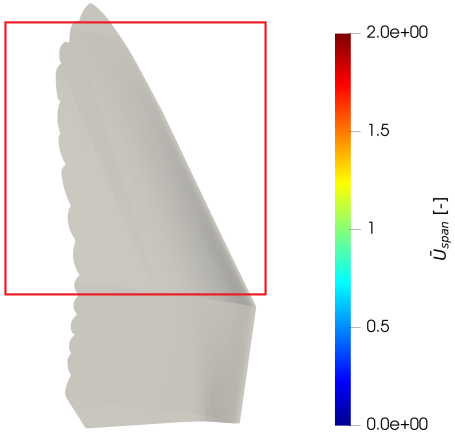

(a) Zoomed out view of the wing with location detail in red frame, color bar is valid for (b),(c) and (d)

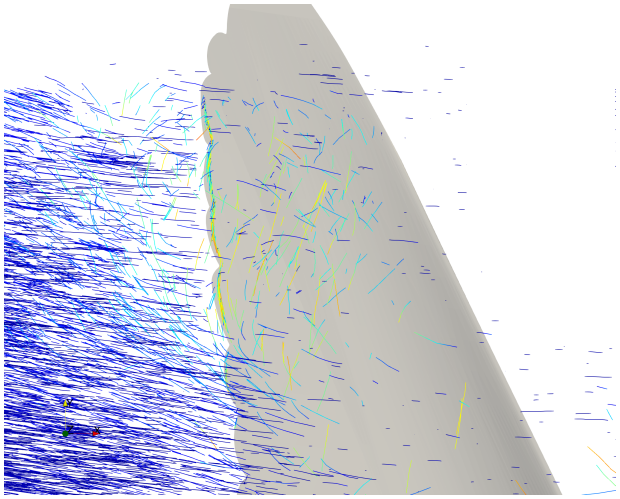

(b) St = 0.19

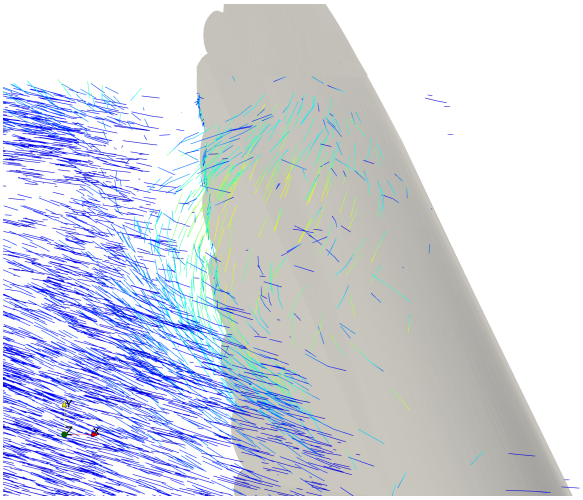

(c) St = 0.24

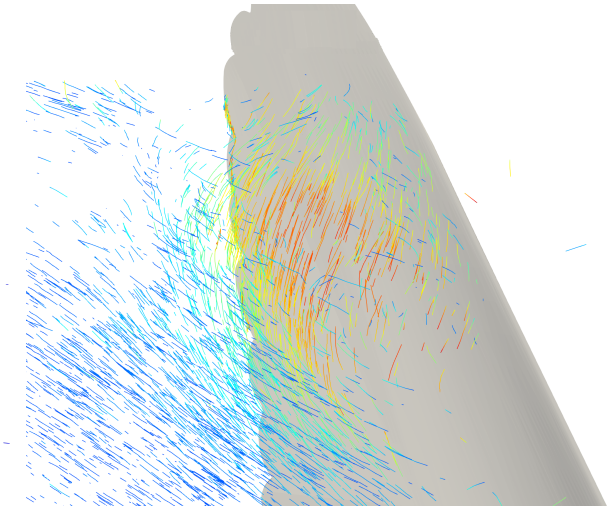

(d) St = 0.33

Fig. 4 Flow field in volume below wing. Particle tracks have length of 5 timesteps. Tracks are plotted for t/T = 0 during the upstroke for three different Strouhal numbers:(b) St = 0.19 (c) St = 0.24 (d) St = 0.33

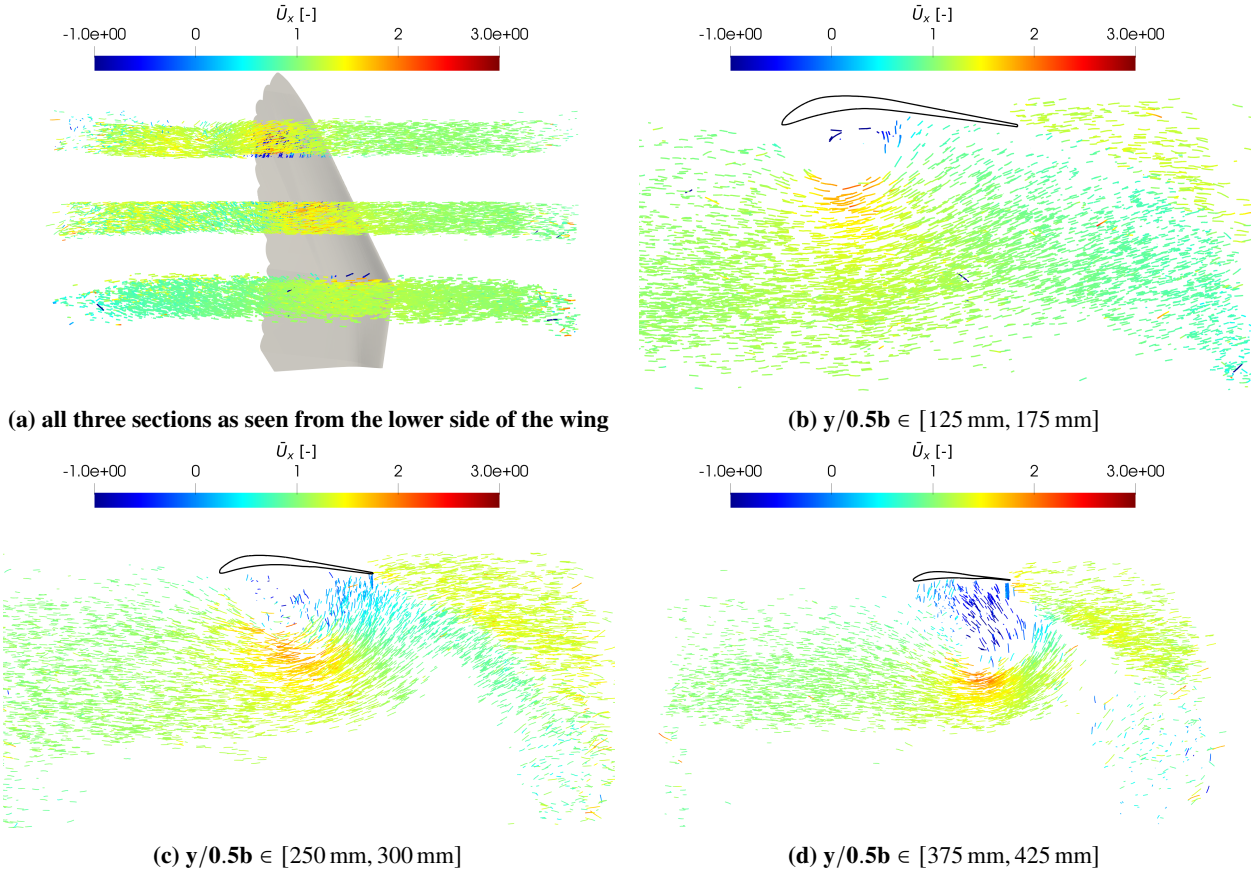

(a) all three sections as seen from the lower side of the wing

(b) y/0.5b $\in$ [125 mm, 175 mm]

(c) y/0.5b $\in$ [250 mm, 300 mm]

(d) y/0.5b $\in$ [375 mm, 425 mm]

Fig. 5 Sectioned view of particle tracks for St = 0.33 during the upstroke at $t/T = 0$. Particle tracks have a length of 5 timesteps.

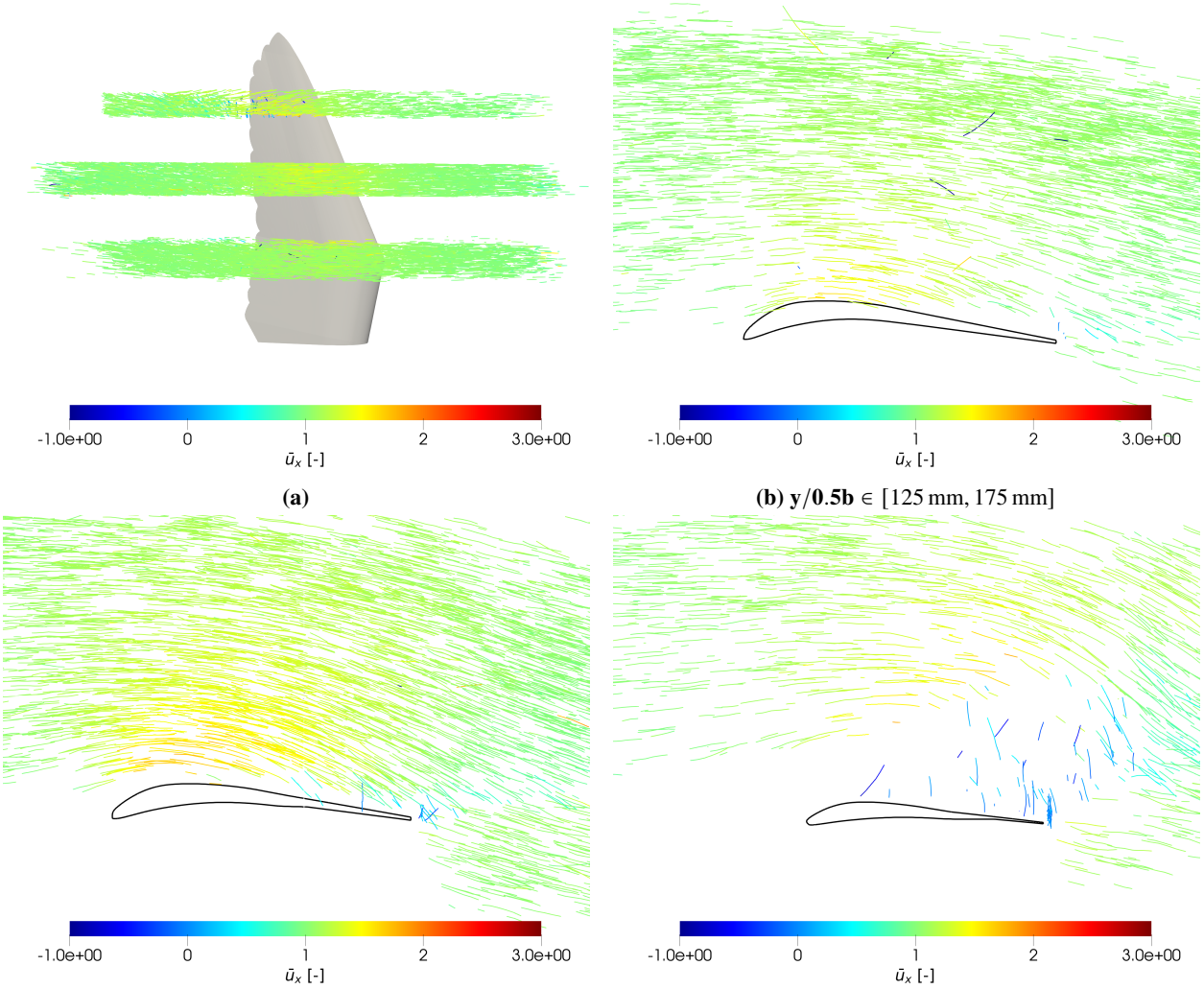

(a)

(b) $\mathbf{y/0.5b} \in [125\,\text{mm}, 175\,\text{mm}]$

(c) $\mathbf{y/0.5b} \in [250\,\text{mm}, 300\,\text{mm}]$

(d) $\mathbf{y/0.5b} \in [250\,\text{mm}, 300\,\text{mm}]$

Fig. 6 Sectioned view of particle tracks for St=0.25 during the downstroke at t/T=0.5. Particle tracks have a length of 5 timesteps.

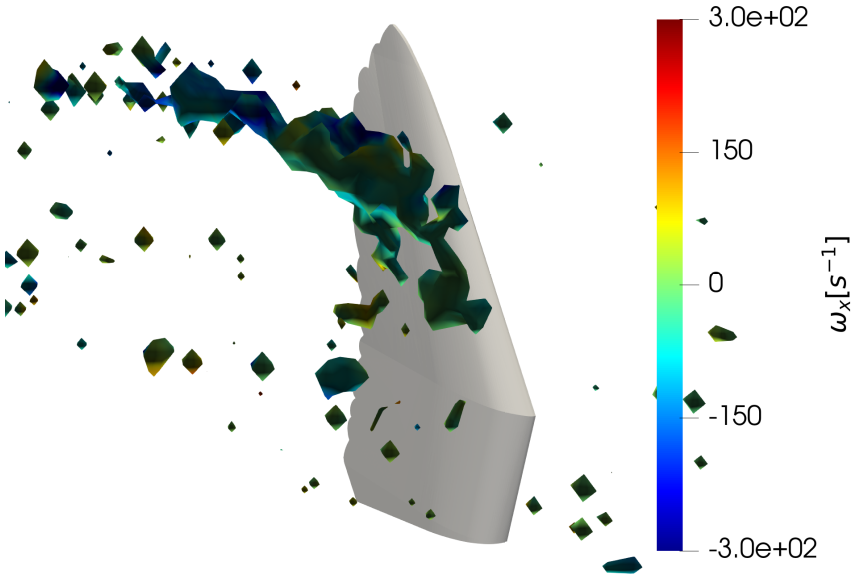

Fig. 7 Isosurface of the λ_2-criterion at $\lambda_2 = 5000$ for St=0.24 during the downstroke at t/T = 0.5. Surface is colored by streamwise vorticity ω_x.

IV. Conclusion and Outlook

The formation of a LEV on the lower side of a robird wing during its upstroke is in line with results from previous 2D uRANS simulations performed on a Robird-like airfoil. The high spanwise velocity could be a sign that this vortex is indeed moving with the wing, as a significant spanwise flow is known to stabilize leading edge vortices. It is not clear if such a structure forming at the lower side of the wing is beneficial. Leading edge vortices are known to enhance lift when attached to the upper side of the wing. Inversely, such a structure that is attached to the lower side of a wing should decrease lift. This raises the question if same structure is present during the free-flight of the Robird. One important difference between free flight conditions and this experiment is the body angle of attack. The Robird flies at a slight angle of attack, whereas this experiment is performed at zero angle of attack. This difference may be significant, as the formation of an LEV is widely believed to be related to the effective angle of attack.

The relatively low seeding density inherent to PTV made it more difficult to interpret the flow on upper side of the wing. It is not quite certain if the flow exhibits a leading edge vortex. Especially noteworthy is that either an LEV or flow detachment is to be expected for St=0.33, but this was not observed. This too could be related to the relatively low seeding density, combined with relatively low amount of particles tracked. In addition, the absence of force measurements makes it difficult to quantify the effects of both structures on the lift and drag generated by the flapping wing. Future work will have to incorporate simultaneous force measurements and PIV measurements on the surface of the flapping wing to further clarify what flow phenomena are present and how they affect the forces generated by the flapping wing.

Acknowledgments

The authors wish to thank W. Lette, E. Öztürk, S. Wanrooy, G. van and E. Leusink for assisting with all technical and practical aspects of the project. This work was supported by the PortWings project funded by the European Research Council [Grant Agreement No. 787675].

References

[1] Folkertsma, G. A., Straatman, W., Nijenhuis, N., Venner, C. H., and Stramigioli, S., "Robird: A Robotic Bird of Prey," *IEEE Robotics and Automation Magazine*, Vol. 24, No. 3, 2017, pp. 22–29. https://doi.org/10.1109/MRA.2016.2636368.

[2] Lentink, D., *Exploring the biofluiddynamics of swimming andflight*, 2008. URL http://library.wur.nl/WebQuery/clc/1894448.

[3] Wood, R. J., "The first takeoff of a biologically inspired at-scale robotic insect," *IEEE Transactions on Robotics*, Vol. 24, No. 2, 2008, pp. 341–347. https://doi.org/10.1109/TRO.2008.916997.

[4] Taylor, G. K., Nudds, R. L., and Thomas, A. L., "Flying and swimming animals cruise at a Strouhal number tuned for high power efficiency," *Nature*, Vol. 425, No. 6959, 2003, pp. 707–711. https://doi.org/10.1038/nature02000.

[5] Festo, "SmartBird: Bird flight deciphered," , 2011. URL https://www.festo.com/group/en/cms/10238.htm.

[6] Gerdes, J., Holness, A., Perez-Rosado, A., Roberts, L., Greisinger, A., Barnett, E., Kempny, J., Lingam, D., Yeh, C. H., Bruck, H. A., and Gupta, S. K., "Robo Raven: A Flapping-Wing Air Vehicle with Highly Compliant and Independently Controlled Wings," *Soft Robotics*, Vol. 1, No. 4, 2014, pp. 275–288. https://doi.org/10.1089/soro.2014.0019.

[7] Ellington, C. P., Van Berg, C. D., Willmott, A. P., and Thomas, A. L., "Leading-edge vortices in insect flight," *Nature*, Vol. 384, No. 6610, 1996, pp. 626–630. https://doi.org/10.1038/384626a0.

[8] Usherwood, J. R., and Ellington, C. P., "The aerodynamics of revolving wings I. Model hawkmoth wings," *Journal of Experimental Biology*, Vol. 205, No. 11, 2002, pp. 1547–1564. https://doi.org/10.1242/jeb.205.11.1547.

[9] Lentink, D., and Dickinson, M. H., "Rotational accelerations stabilize leading edge vortices on revolving fly wings," *Journal of Experimental Biology*, Vol. 212, No. 16, 2009, pp. 2705–2719. https://doi.org/10.1242/jeb.022269.

[10] Chin, D. D., and Lentink, D., "Flapping wing aerodynamics: From insects to vertebrates," *Journal of Experimental Biology*, Vol. 219, No. 7, 2016, pp. 920–932. https://doi.org/10.1242/jeb.042317.

[11] Warrick, D. R., Tobalske, B. W., and Powers, D. R., "Aerodynamics of the hovering hummingbird," *Nature*, Vol. 435, No. 7045, 2005, pp. 1094–1097. https://doi.org/10.1038/nature03647.

[12] Muijres, F. T., Johansson, L. C., and Hedenström, A., "Leading edge vortex in a slow-flying passerine," *Biology Letters*, Vol. 8, No. 4, 2012, pp. 554–557. https://doi.org/10.1098/rsbl.2012.0130.

[13] Muijres, F. T., Christoffer Johansson, L., Winter, Y., and Hedenström, A., "Leading edge vortices in lesser long-nosed bats occurring at slow but not fast flight speeds," *Bioinspiration and Biomimetics*, Vol. 9, No. 2, 2014. https://doi.org/10.1088/1748-3182/9/2/025006.

[14] Hubel, T. Y., and Tropea, C., "The importance of leading edge vortices under simplified flapping flight conditions at the size scale of birds," *Journal of Experimental Biology*, Vol. 213, No. 11, 2010, pp. 1930–1939. https://doi.org/10.1242/jeb.040857.

[15] Mulder, J. L., and Hoeijmakers, H. W. M., "Computational and experimental investigation into flapping wing propulsion," *54th AIAA Aerospace Sciences Meeting*, Vol. 0, No. January, 2016, pp. 1–33. https://doi.org/10.2514/6.2016-0802.

[16] Groot Koerkamp, L., de Santana, L. D., Hoeijmakers, H. W. M., and Venner, K. H., "Investigation into Wake of Flapping Wing of Robotic Bird," *AIAA Aviation 2019 Forum*, American Institute of Aeronautics and Astronautics, Reston, Virginia, 2019. https://doi.org/10.2514/6.2019-3582, URL https://arc.aiaa.org/doi/10.2514/6.2019-3582.

[17] Groot Koerkamp, L., de Santana, L. D., Hoeijmakers, H. W. M., Venner, C., and Stramigioli, S., "Development and experimental validation of lifting line-based model for a Robotic Falcon," *AIAA AVIATION 2022 Forum*, American Institute of Aeronautics and Astronautics, Reston, Virginia, 2022. https://doi.org/10.2514/6.2022-3447, URL https://arc.aiaa.org/doi/10.2514/6.2022-3447.

[18] Scarano, F., "Tomographic PIV: Principles and practice," *Measurement Science and Technology*, Vol. 24, No. 1, 2013. https://doi.org/10.1088/0957-0233/24/1/012001.

[19] Caridi, G. C. A., Ragni, D., Sciacchitano, A., and Scarano, F., "HFSB-seeding for large-scale tomographic PIV in wind tunnels," *Experiments in Fluids*, Vol. 57, No. 12, 2016, pp. 1–13. https://doi.org/10.1007/s00348-016-2277-7.

[20] Schneiders, J. F. G., "Open Aircraft Performance Modeling Based on an Analysis of Aircraft Surveillance Data," Ph.D. thesis, TU Delft, 2017. https://doi.org/10.4233/uuid:244b9699-0814-4bc9-aa48-07361989bd64.

[21] Schanz, D., Schröder, A., Gesemann, S., Michaelis, D., and Wieneke, B., "' Shake The Box ': A highly efficient and accurate Tomographic Particle Tracking Velocimetry (TOMO-PTV) method using prediction of particle positions," *10th International Symposium on Particle Image Velocimetry - PIV13. Delft, The Netherlands, July 1-3.*, 2013, pp. 1–13.

[22] Schanz, D., Gesemann, S., and Schröder, A., "Shake-The-Box: Lagrangian particle tracking at high particle image densities," *Experiments in Fluids*, Vol. 57, No. 5, 2016, pp. 1–27. https://doi.org/10.1007/s00348-016-2157-1.

[23] de Santana, L. D., Sanders, M. P., Venner, C. H., and Hoeijmakers, H. W. M., "The UTwente Aeroacoustic Wind Tunnel Upgrade," *2018 AIAA/CEAS Aeroacoustics Conference*, American Institute of Aeronautics and Astronautics, Reston, Virginia, 2018. https://doi.org/10.2514/6.2018-3136, URL https://arc.aiaa.org/doi/10.2514/6.2018-3136.

[24] Jeong, J., and Hussain, F., "On the identification of a vortex," *Journal of Fluid Mechanics*, Vol. 285, 1995, pp. 69–94. https://doi.org/10.1017/S0022112095000462.